Optical anisotropy in 5-nm-scale T-shaped quantum wires fabricated by the cleaved-edge overgrowth method

Hidefumi Akiyama, Takao Someya, and Hiroyuki Sakaki
PRESTO and Quantum Transition Project, Research Development Corporation of Japan, and Research Center for Advanced Science and Technology,University of Tokyo, 4-6-1 Komaba, Meguro-ku, Tokyo 153, Japan
(Received 23 October 1995; revised manuscripti received 4 December 1995)

Optical anisotropy has been evaluated in terms of polarization dependence of photoluminescence (PL) and PL excitation (PLE) spectra for 5-nm-scale GaAs/AlAs T-shaped quantum wires (T-QWR's). They were prepared by the cleaved-edge overgrowth method, and their potential profile was previously characterized by spatially resolved PL measurements. The PL and PLE signals for T-QWR's showed stronger polarization along the T-QWR's. Comparing T-QWR's with a reference QW grown on a (110) surface, we clarified the optical anisotropy induced purely by the lateral confinement in T-QWR's.

Optical anisotropy, i.e., the polarization dependence of optical absorption and/or emission, has been one of the main subjects in quantum wires[1,2] (QWR's) and other modulated semiconductor structures, because it directly reflects the anisotropic electronic states inherent to each structure. In GaAs, the optical anisotropy is caused mainly by the anisotropic electronic states at the top of valence bands, which have total angular momentum of $j=3/2$.

In fact, for most types of GaAs QWR structures so far reported, the polarization dependence of photoluminescence (PL) and PL excitation (PLE) spectra has been presented as a proof of the electronic states resulting from lateral confinement.[3–10] However, it has been difficult to experimentally evaluate the optical anisotropy introduced purely by the lateral confinement in QWR's, which has been predicted by theories.[11–13]

This is, first, because the optical anisotropy is also caused by the valence-band anisotropy due to warping distortion, uniaxial strain, or anisotropic perturbation potential of anisotropic interface roughness.[14] In addition, for QWR's grown on patterned substrates, the anisotropy in macroscopic sample geometry can induce additional polarization dependence of their PL and PLE spectra. Furthermore, for small QWR's below 10-nm scale, which are of our current interest, the PL or PLE peaks tend to broaden and overlap with other spectral structures, which makes it difficult to quantify the optical anisotropy from the PL and PLE spectra. For quantitative analysis of the observed anisotropy, one must accurately characterize both the potential profile and the quantized energy levels of QWR's, which is often difficult. For these reasons, the quantitative investigation of the optical anisotropy in reference to the confinement potential profile in small QWR's of 5-nm scale has never been accomplished completely.

We report, in this paper, the optical anisotropy measured in terms of the polarization dependence of PL and PLE in 5-nm scale T-shaped QWR's (T-QWR's) and a reference QW grown on a (110) surface. Clear optical anisotropy was observed for the T-QWR's, as well as the constituent adjacent QW's forming T structures and the reference (110) QW. Comparing the observed optical anisotropy for the T-QWR's and the reference QW, we evaluated the optical anisotropy induced by the lateral confinement in T-QWR's.

The high-quality T-QWR sample studied here was fabricated by the cleaved edge overgrowth (CEO) method[15] with molecular beam epitaxy (MBE). The confinement potential of QWR's has been well characterized by spatially resolved micro-PL measurements. The details are described in separate papers.[16,17]

Figure 1(a) shows the schematic structure of our T-QWR sample and the experimental geometry. The T-QWR's are formed at the intersection of multiple QW's (denoted as QW1) grown in the first MBE growth and a QW

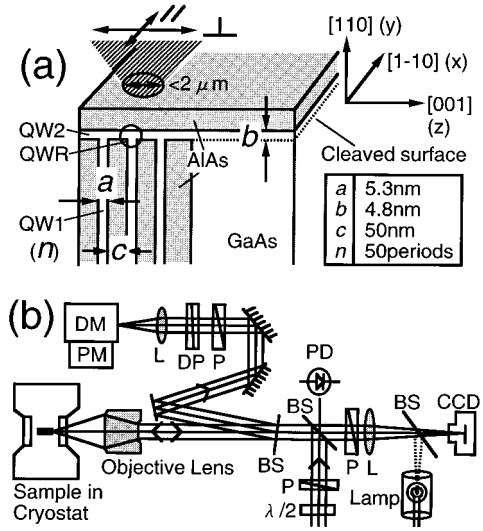

FIG. 1. (a) Geometry of structure, crystal orientation, and polarization, with the definition of x, y, and z directions, in the 5-nm-scale GaAs/AlAs T-QWR sample fabricated by the cleaved edge overgrowth method. (b) Schematic of micro-PL setup. DM, double-monochromator; PM, photomultiplier; L, lens; P, polarizer; DP, depolarizer; PD, photodiode; BS, beam splitter; λ/2, half-wave retarder.

(denoted as QW2) overgrown as the second MBE growth after *in situ* cleavage. The multiple QW structure consists of $n=50$ periods of GaAs QW's (QW1; thickness $a=5.3$ nm) (Ref. 18) and AlAs barriers (thickness $c=50$ nm). The overgrown QW is of a GaAs layer (QW2; thickness $b=4.8$ nm),[18] covered by an AlAs barrier layer. For later discussions, we define the [001] (the first growth direction) as the z direction, the [110] (the overgrowth direction) as the y direction, and the [1-10] (the QWR direction) as the x direction, as shown in the figure. We also denote polarization along [1-10] ([001]) as $\parallel$ ($\perp$), since [1-10] ([001]) is parallel (perpendicular) to the T-QWR's and the QW1 layers.

From the micro-PL measurements,[16,17] the energy levels of those structures at 4 K were precisely determined as PL photon energy of respective peaks. They were 1.633 eV for T-QWR, 1.668 eV for QW1, and 1.680 eV for QW2.[18] The effective lateral confinement energy defined as the energy difference between T-QWR and QW1 (in this sample, since QW1 had lower energy than QW2) was 35 meV, which was larger than the thermal energy $k_BT\sim 26$ meV at room temperature.

For this sample, we performed polarization-dependent PL and PLE measurements with a cw titanium sapphire (TiS) laser and a conventional micro-PL setup shown in Fig. 1(b). The PL was detected via the (110) surface in the backward scattering geometry. The output light of the TiS laser was horizontally or perpendicularly polarized with a Fresnel-rhomb half-wave retarder and a Glan-Thomson prism. It was then partly reflected by a beam splitter placed at 45° and focused, in the normal-incidence configuration, into a less-than-2-μm spot on the sample at 4 K in a cryostat (Oxford Instruments CF2102), which was monitored by CCD camera system. An objective lens for the near-infrared region (Mitsutoyo M Plan NIR 50x), with nominal magnification factor of 50, working distance of 17 mm, and numerical aperture of 0.42, was used. The PL was collected by the same objective lens, partly reflected by another beam splitter placed at nearly 0° and led to a 10-cm double monochromator with a GaAs photomultiplier. The signal was measured with the lock-in detection technique. A polarizer and a depolarizer were placed in front of the monochromator to analyze the polarization of the PL. The polarization dependence of PL and PLE was measurable by the usage of the depolarizer, near-infrared broad-band optics for all the polarization-sensitive elements, and the normal incidence configuration both at the sample and the second beam splitter.

Figure 2 shows PL (a) and PLE (b) of the T-QWR sample at 4 K. The two peaks in the PL spectra (a) are assigned to the lowest-energy excitons in T-QWR and QW1. In QWR's and QW's, the $j=3/2$ hole states are separated into heavy-hole (HH) and light-hole (LH) states. Optical transitions from these states to a conduction-electron state are observed as separate exciton absorption peaks. In this paper, we use the term HH (LH) in the sense that it has heavier (lighter) effective mass than the other in the direction of the confinement of QW's and QWR's. Thus, the lowest-energy excitons in QWR's and QW1 are those composed of HH having lower optical transition energy than LH due to smaller quantization energy. The photon energy of the excitation laser was 1.72 eV, and the excitation power was 0.2 mW. Thus, the excitation light is partly absorbed in QWR and QW2, but mostly in

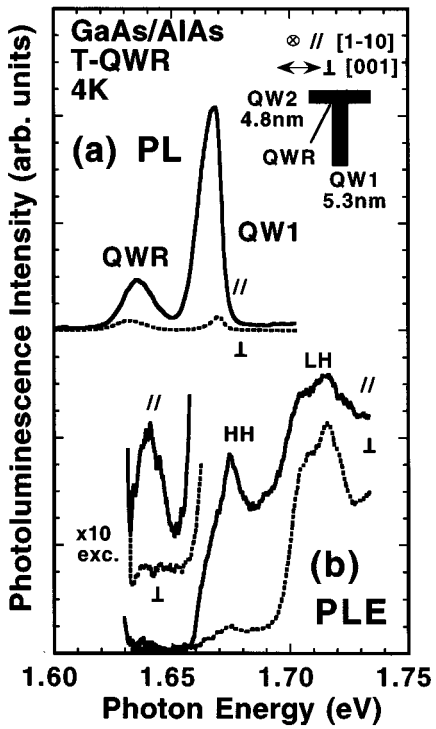

FIG. 2. PL (a) and PLE (b) spectra measured at 4 K for the 5-nm-scale GaAs/AlAs T-QWR sample. The polarization of the light for detection in PL and excitation in PLE was parallel ($\parallel$, solid curves) or perpendicular ($\perp$, broken curves) to the QWR's. The excitation laser energy was 1.72 eV in PL measurements. The detection energy in PLE measurements was 1.625 eV, which is at the low energy tail of QWR. The magnified PLE spectra were measured with 10 times higher excitation intensity.

QW1. However, the PL intensity of T-QWR's is comparable with that of QW1, since the electrons and holes generated in QW1 flow into QWR, which dominates the PL of QWR's.

Strong polarization anisotropy was observed when the polarization of PL was analyzed. The solid (broken) curve shows PL with $\parallel$ ($\perp$), that is, polarization parallel (perpendicular) to the QWR's and the QW1 layers. The PL signal ratio $I_\perp/I_\parallel$ between the two polarizations was 20% for QWR's, and was 6% for QW1, which we will discuss later. When the polarization of the excitation light was changed from parallel to perpendicular to the QWR, there was no change in the PL spectral shape, that is, no polarization memory, at this excitation energy.

Then, we performed PLE measurements of QWR by setting the detection energy at the low-energy tail (1.625 eV) of QWR PL for the polarization of excitation light parallel ($\parallel$, solid curves) and perpendicular ($\perp$, broken curves) to the QWR's, as shown in Fig. 2(b). In the PLE spectra, there exist not only structures arising from the QWR but also the QW1 above 1.66 eV. The large structure of QW1 in the PLE is caused by a plentiful carrier flow from QW1 to QWR. The structure of QW2 was not observed since it is located at a higher-energy region than that of QW1 and is overlapped with the much larger structure of QW1.

The overall spectra were measured with the excitation power of 0.2 mW, whereas the magnified spectra near the detection energy were measured with 2 mW power. For all

the pairs of data for both polarizations in Fig. 2, the detection sensitivity and the excitation intensity were kept constant. We expect that the possible experimental error in determining relative signal intensity I is about 10% or less. Thus, we can compare the relative peak intensity for both polarizations to evaluate the optical anisotropy. The (110) surfaces through which PL was detected were smooth and flat without patterns causing an additional macroscopic geometrical effect. Therefore, the anisotropy directly shows the anisotropic electronic states, or valence-band states, in the lowest-energy excitons in QWR's and in QW1.

Before discussing the optical anisotropy, we should note the small Stokes shift and the sharp PL and PLE spectra. The values of the PL linewidth and the Stokes shift are 15 meV and 5 meV for QWR's, respectively, and 10 meV and 7 meV for QW1. These small values demonstrate the high quality of the sample, and thus support the reliability of our quantitative discussion.

The large PLE structures above 1.66 eV in Fig. 2(b) are due to the HH and LH excitons in QW1. The optical anisotropy of QW1 agrees well with the well-known optical anisotropy of standard (001) QW's observed from the (110) cleaved surface;[19] the HH and LH states in QW1 are mainly of Bloch states $(1/\sqrt{2})|(X\pm iY)^{\uparrow}_{\downarrow}\rangle$ and $-\sqrt{(2/3)}|Z^{\uparrow}_{\downarrow}\rangle \pm(1/\sqrt{6})|(X\pm iY)^{\downarrow}_{\uparrow}\rangle$ in Bastard's notation[20] with z component of angular momentum $j_z=\pm 3/2$ and $\pm 1/2$, respectively, such that the relative optical transition intensities in the (001) QW's are calculated as 0, 3, 4, and 1 for $I_{\mathrm{HH},\perp(z)}$, $I_{\mathrm{HH},\parallel(x)}$, $I_{\mathrm{LH},\perp(z)}$, and $I_{\mathrm{LH},\parallel(x)}$, respectively. In reality, the forbidden transition of HH with $\perp$ polarization can be weakly observed. The observed PLE intensity $I_{\mathrm{HH},\perp}$ was about 14% of $I_{\mathrm{HH},\parallel}$, which is in fair agreement with the PL data of 6%. Reasonable agreement was obtained among the previous reports,[19] the model calculation, and the present observation for the (001) QW, which supports the validity and the reliability of the following quantitative study of optical anisotropy on QWR's.

As for QWR's, Fig. 2(b) shows the PLE signal ratio $I_{\perp}/I_{\parallel}\simeq 39\%$. Since there is some contribution of the smearing tail structures of the QW1 and the stray light, the estimation requires a proper extraction of this contribution. The value is obtained from the comparison of the peak intensity ratio, because peak heights are least affected by the additional contribution of the tail structures. The value is again in fair agreement with the PL data of 20%.

To look into the optical anisotropy of QWR, we need to compare the data with those of the reference QW on a (110) surface to separate the optical anisotropy due to the crystallographic anisotropy.[21] Figure 3 shows PL (a) and PLE (b) at 4 K of the reference GaAs/$Al_{0.3}Ga_{0.7}As$ QW of 5.4 nm thickness formed on a (110) surface. The solid and broken curves are for polarization $\parallel$ (along [1-10]) and $\perp$ (along [001]), respectively. The peak in the PL spectra is of HH excitons, whereas the two PLE peaks are of HH excitons and LH excitons. Due to the crystallographic anisotropy, optical anisotropy was observed in the HH exciton transitions between $\parallel$ and $\perp$ polarization. The signal ratio $I_{\perp}/I_{\parallel}$ was 60% in the PL peaks, and was 67% in the PLE, showing good agreement with each other.

The results of optical anisotropy obtained from Figs. 2 and 3 are summarized in Table I. Though the values of

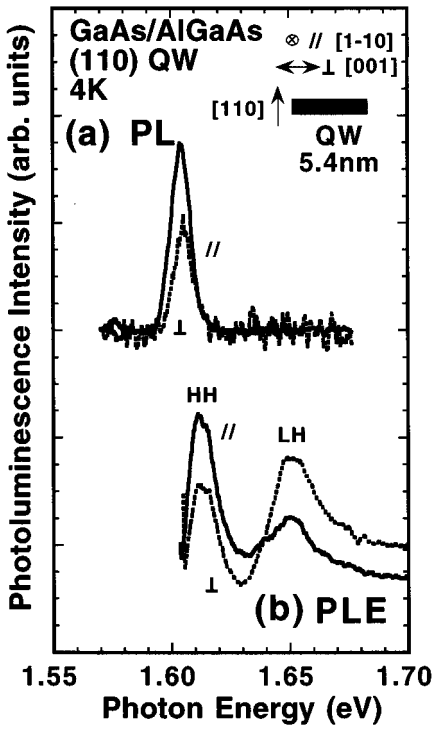

FIG. 3. PL (a) and PLE (b) spectra measured at 4 K for the reference (110) QW in the same geometry as in Fig. 2.

$I_{\perp}/I_{\parallel}$ tend to be smaller for the PL data than for the PLE data, we found a clear difference between the results for the QWR and the reference (110) QW, which is ascribed to the optical anisotropy resulting purely from the lateral confinement in QWR's. To get some insight into the results, we compare them with some model calculations in the following way.

We start from the simplest model with axial symmetry along the x direction, neglecting crystal band anisotropy and the asymmetric shape of QWR; the HH state in QWR is then of Bloch states $-\sqrt{(2/3)}|X^{\uparrow}_{\downarrow}\rangle\pm(1/\sqrt{6})|(Y\pm iZ)^{\downarrow}_{\uparrow}\rangle$ with x component of angular momentum $j_x=\pm 1/2$, which gives the relative optical transition intensities of 1:4 for $I_{\mathrm{HH},\perp(z)}$: $I_{\mathrm{HH},\parallel(x)}$, that is, $I_{\perp}/I_{\parallel}=25\%$. In this case, we obtain $I_{\perp}/I_{\parallel}(=I_{[001]}/I_{[1-10]})=100\%$ for the reference (110) QW.

When we introduce crystallographic anisotropy, however, the other j_x states are mixed, which modifies the optical anisotropy. To see this effect, the crystal band anisotropy was taken into account under the approximation of infinite barri-

TABLE I. Optical anisotropy $I_{\perp}/I_{\parallel}$, that is $I_{[001]}/I_{[1-10]}$, for heavy-hole exciton transition in T-QWR, reference (110) QW, and QW1 evaluated via PL, PLE, and theories assuming anisotropic and isotropic valence-band structures.

Sample	PLE (%)	PL (%)	Theory (%) (anisotropic)	Theory (%) (isotropic)
QWR	39	20	34	25
(110) QW	67	60	86	100
QW1	14	6	0	0

ers and cylindrical shape.[22,23] According to the results of Yamaguchi and co-workers,[23] the optical anisotropy ratio $I_{\perp}/I_{\parallel}$ is 34% for the QWR, whereas for the reference (110) QW it is $I_{\perp}/I_{\parallel}(=I_{[001]}/I_{[1-10]})=86\%$. It is interesting to point out that the optical anisotropy ratio is decreased in the (110) QW, while it is increased in the QWR.

These values are compared with the experimental results in Table I. In spite of the obvious difference in the shape between cylindrical rods and the T-QWR's, we find a good agreement between the model calculation and the experiment. This may be because of a comparable confinement in y and z directions in the T-QWR's. To reproduce the optical anisotropy precisely, a more rigorous theory is required.

In conclusion, we measured the optical anisotropy of the 5-nm-scale GaAs/AlAs T-QWR sample prepared by the cleaved edge overgrowth method. Its energy-level profile was well characterized by spatially resolved PL measurements, showing the lateral confinement energy as large as 35 meV. The PL and PLE signals for T-QWR's were found to be more polarized along the T-QWR's. The optical anisotropy induced purely by the confinement potential in T-QWR's was evaluated via the comparison between the T-QWR's and the reference (110) QW. These results showed good agreement with a simple theory considering only the crystal band anisotropy.

The authors would like to thank Dr. Yamaguchi (NEC) for helpful discussions. This work is partly supported by a Grant-in-Aid from the Ministry of Education, Science, Sports, and Culture, Japan.

[1] H. Sakaki, Jpn. J. Appl. Phys. **19**, L735 (1980).
[2] Y. Arakawa and H. Sakaki, Appl. Phys. Lett. **40**, 939 (1982).
[3] M. Tsuchiya, J. M. Gaines, R. H. Yan, R. J. Simes, P. O. Holtz, L. A. Coldren, and P. M. Petroff, Phys. Rev. Lett. **62**, 466 (1989); H. Weman, M. S. Miller, and J. L. Merz, Phys. Rev. Lett. **68**, 3656 (1992).
[4] M. Tanaka and H. Sakaki, Appl. Phys. Lett. **54**, 1326 (1989).
[5] D. Gershoni, J. S. Weiner, S. N. G. Chu, G. A. Baraff, J. M. Vandenberg, L. N. Pfeiffer, K. West, R. A. Logan, and T. Tanbun-Ek, Phys. Rev. Lett. **65**, 1631 (1990).
[6] A. R. Goñi, L. N. Pfeiffer, K. West, A. Pinczuk, H. U. Baranger, and H. L. Störmer, Appl. Phys. Lett. **61**, 1956 (1992).
[7] E. Kapon, K. Kash, E. M. Clausen, Jr., D. M. Hwang, and E. Colas, Appl. Phys. Lett. **60**, 477 (1992).
[8] H. Kanbe, A. Chavez-Pirson, H. Ando, H. Saito, and T. Fukui, Appl. Phys. Lett. **58**, 2969 (1991).
[9] H. Weman, M. S. Miller, C. E. Pryor, Y. J. Li, P. Bergman, P. M. Petroff, and J. L. Merz, Phys. Rev. B **48**, 8047 (1993).
[10] J. Bloch U. Bockelmann, and F. Laruelle, Solid State Electron. **37**, 529 (1994).
[11] P. C. Sercal and K. J. Vahara, Appl. Phys. Lett. **57**, 545 (1990).
[12] D. S. Citrin and Y.-C. Chang, Phys. Rev. B **43**, 11 703 (1991).
[13] H. Ando S. Nojima, and H. Kanbe, J. Appl. Phys. **74**, 6383 (1993).
[14] G. E. W. Bauer and H. Sakaki, Surf. Sci. **267**, 442 (1992).
[15] L. N. Pfeiffer, K. West, H. L. Störmer, J. P. Eisenstein, K. W. Baldwin, D. Gershoni, and J. Spector, Appl. Phys. Lett. **56**, 1697 (1990).
[16] T. Someya, H. Akiyama, and H. Sakaki, Appl. Phys. Lett. **66**, 3672 (1995).
[17] T. Someya, H. Akiyama, and H. Sakaki, J. Appl. Phys. (to be published).
[18] The T-QWR sample used is the same as that used in Refs. 16 and 17. The well thicknesses a and b have been determined in Ref. 17 by comparing the PL data with calculated energy levels of QW's.
[19] J. S. Weiner, D. S. Chemla, D. A. B. Miller, H. A. Haus, A. C. Gossard, W. Wiegmann, and C. A. Burrus, Appl. Phys. Lett. **47**, 664 (1985).
[20] G. Bastard, *Wave Mechanics Applied to Semiconductor Heterostructures* (Halsted Press, New York, 1988).
[21] D. Gershoni, I. Brener, G. A. Baraff, S. N. G. Chu, L. N. Pfeiffer, and K. West, Phys. Rev. B **44**, 1930 (1991).
[22] C. R. McIntyre and L. J. Sham, Phys. Rev. B **45**, 9443 (1992).
[23] A. A. Yamaguchi and A. Usui, J. Appl. Phys. **78**, 1361 (1995); A. A. Yamaguchi, K. Nishi, and A. Usui, Jpn. J. Appl. Phys. **33**, L912 (1994).